

Using MPPT in Multi-Pulse Converters for Photovoltaic Cogeneration

Lucas Lapolli Brighenti, Rubens Tadeu Jr Hock, Luis Gustavo Kremer, Alessandro Luiz Batschauer, Marcello Mezaroba

Electrical Power Processing Group - nPEE
 Santa Catarina State University - UDESC
 Joinville, Brazil

lucasbrighenti@msn.com, rubenshockjr@gmail.com, lgkremer@hotmail.com, alessandrobatschauer@gmail.com,
marcello.mezaroba@udesc.br

Abstract—One alternative for the processing of energy acquired by photovoltaic panels is the use of phase-controlled inverters associated with multi-pulse autotransformers, which is nothing more than a dual system for multi-pulse rectifiers. This converter has advantages related to robustness, low maintenance, reliability and low cost. Another important feature is that the use of transformers with specific displacement reduces the quantity of harmonic current injected into the grid. This paper will present this converter and proposes the use of Maximum Power Point Tracking (MPPT) acting on the average input voltage of the inverter, using the trigger angle to vary the average voltage of the converter and keep it operating at the maximum power point of the PV panels.

Keywords—Autotransformer, Phase-controlled inverters, Photovoltaic cogeneration, SCR, Y-differential connection.

I. INTRODUCTION

This project proposes the usage of multi-pulse converters associated to autotransformers with differential connection applied to photovoltaic cogeneration. References [1] and [2] present topologies of multi-pulse converters with isolated transformers. The choice for autotransformers has as a main objective to reduce cost and increase the system's efficiency, the general scheme of the project is presented at Figure 1.

Passive rectifiers that present a unitary power factor with a low output voltage ripple have been already presented on literature [3] and [4]. These rectifiers are known as multi-pulse converters. References [5] and [6] present some configurations of multi-pulse rectifiers using an autotransformer with differential connections.

A Graetz Bridge rectifier is known as a 6 pulse rectifier, in case it presents a constant current with no ripple at the DC output, the pair and multiple of 3 harmonics are naturally eliminated due to the symmetry of the current's waveform. Using thyristors or silicon controlled rectifier (SCR) instead

of diodes, it is possible to allow this converter to operate on all four quadrants. With trigger angles above 90° it operates as a non-autonomous phase controlled inverter. A 6-pulse converter applied to photovoltaic cogeneration is presented at [7].

It is possible to reduce even more the amount of harmonic content injected on the grid, by the use of association of 6 pulse rectifiers. This way, grid current's harmonics will be of $k.n \pm 1$ orders, where n is the number of pulses of the converter and k is an entire positive number. It is needed $n/6$ rectifiers, which have to be connected to three-phase subsystems, with a $360^\circ/n$ of displacement [6]. On a dual form of the multi-pulse rectifier, it is proposed the usage of phase controlled inverters instead of rectifiers, allowing the possibility of injecting current on the grid. Figure 2 shows the complete schematic of the proposed converter connections.

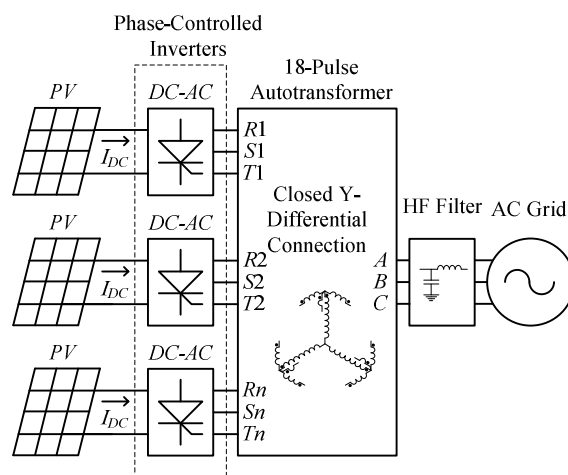


Figure 1. General scheme of the proposed system.

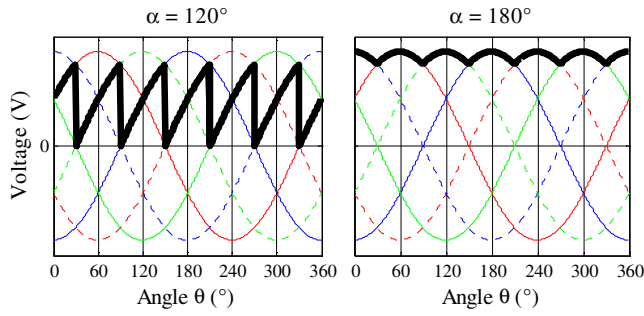


Figure 3. Phase-controlled inverter's input voltage waveform for an angle of 120°(left) and 180°(right).

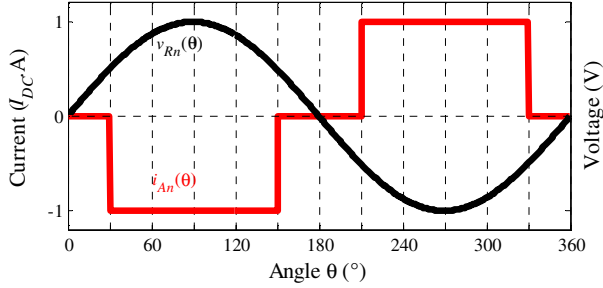


Figure 4. Output voltage and current of non-autonomous inverter's phase R.

III. 18-PULSE AUTOTRANSFORMER

The autotransformer is used to generate the three three-phase subsystems (20° displaced each one), needed to obtain the 18 pulse converter. The autotransformer with closed Y-differential connection was chosen because it presents a lower voltage comparing to the grid's feeding voltage, becoming an attractive choice for photovoltaic systems

The voltage shifts of 20° are created by the combination of the voltage vectors amplitude of the autotransformer's winding. The phasor diagram is presented at Figure 5. The subsystems have gaps of -20°, 0° and +20° in comparison with the grid's voltage.

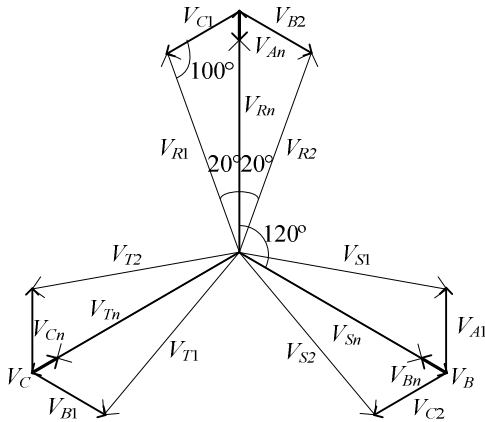


Figure 5. Phasorial diagram of the multi-pulse autotransformer's voltages.

The turn ratios for the secondary windings are obtained from the trigonometric relations presented at TABLE I.

TABLE I. RELATIONS OF TURNS AND VOLTAGE FOR PHASE A

V_{A1}, V_{A2}	$V_A \cdot \sin(20^\circ) / \sin(100^\circ)$	$0.3473 V_A$
V_{An}	$V_A - V_{Rn}$	$0.1206 V_A$
V_{R1}, V_{R2}, V_{Rn}	$V_A \cdot \sin(60^\circ) / \sin(100^\circ)$	$0.8794 V_A$
N_{20°	V_A / V_{A1}	2.8794
N_{0°	V_A / V_{An}	8.2819

Voltages of phases R of the subsystems are presented at Figure 6.

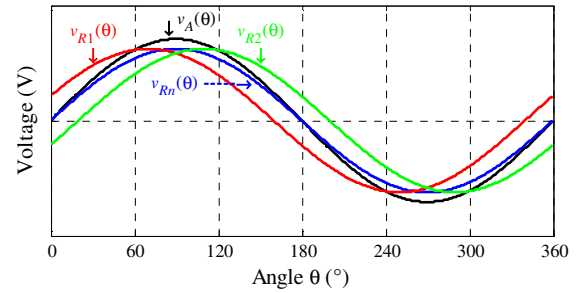


Figure 6. Voltages of phase R of the subsystems generated by the autotransformer.

The current at the secondary windings is the output current of the inverter itself (Figure 4). The primary's current is composed by the sum of the currents referred to the secondary, represented at (2), (3) and (4).

$$i_{LA}(t) = [i_{A1}(t) + i_{A2}(t)] / N_{20^\circ} - i_{An}(t) / N_{0^\circ} \quad (2)$$

$$i_{LB}(t) = [i_{B1}(t) + i_{B2}(t)] / N_{20^\circ} - i_{Bn}(t) / N_{0^\circ} \quad (3)$$

$$i_{LC}(t) = [i_{C1}(t) + i_{C2}(t)] / N_{20^\circ} - i_{Cn}(t) / N_{0^\circ} \quad (4)$$

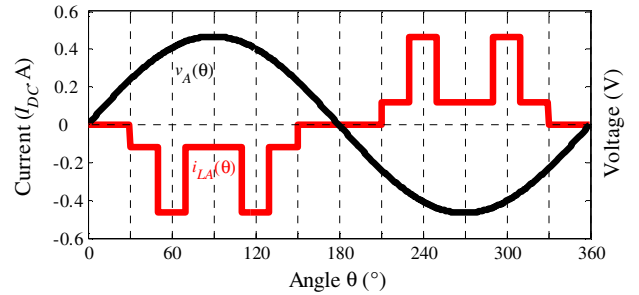


Figure 7. Voltage and current at L_A winding of the autotransformer.

Current injected at the grid is composed by the sum of the currents that enter in the nodes connected to the grid, as shown at Figure 2.

$$i_A(t) = i_{LA}(t) + i_{C1}(t) + i_{B2}(t) + i_{An}(t) \quad (5)$$

$$i_B(t) = i_{LB}(t) + i_{A1}(t) + i_{C2}(t) + i_{Bn}(t) \quad (6)$$

$$i_C(t) = i_{LC}(t) + i_{B1}(t) + i_{A2}(t) + i_{Cn}(t) \quad (7)$$

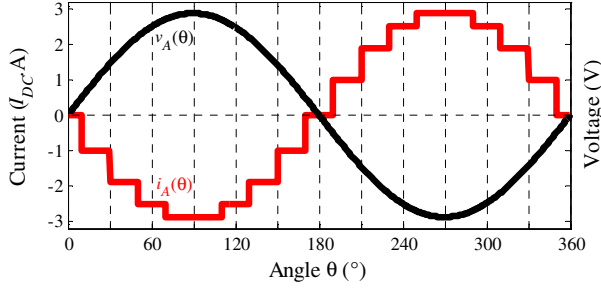


Figure 8. Voltage and current provided to phase A of the grid.

The waveform of current I_A can be decomposed into a Fourier series [8]. Thus, the expressions for current are:

$$i_{An}(\theta) = \sum_{k=1,3,5,\dots}^{\infty} \frac{4I_{DC}}{k\pi} \cos\left(\frac{k\pi}{6}\right) \sin(k\pi \cdot \theta) \quad (8)$$

$$i_A(\theta) = I_{DC} \sum_{k=1,3,5,\dots}^{\infty} \left[\frac{2}{N_{2p}} \cos\left(k \cdot \frac{100}{180} \pi\right) - \frac{1}{N_p} + 2 \cos\left(k \cdot \frac{20}{180} \pi\right) + 1 \right] \cdot \frac{4}{k\pi} \cos\left(k \cdot \frac{30}{180} \pi\right) \cdot \sin[k \cdot (\theta + \alpha)] \quad (9)$$

The output current's total harmonic distortion is 10.05% and the displacement angle between current and voltage is the trigger angle α itself. The power factor is:

$$PF = 0,995 \cdot \cos(\alpha) \quad (10)$$

The power factor for a trigger angle of 120° is 0.498 and the mean voltage is 50% of nominal voltage. Reference [5] shows the power processed by the autotransformer is 21.88% of the converter's nominal input voltage.

IV. PHOTOVOLTAIC PANELS

This section presents an evaluation of the typical behavior of photovoltaic panels. The presented curves are of the SW130 model, manufactured by *Solarword*. Panels of other models and producers presents similar typical curves, but with different voltage, current and power values.

Figure 9 and Figure 10 shows power versus voltage curves in different conditions of temperature and irradiation, the model construction is presented at [9].

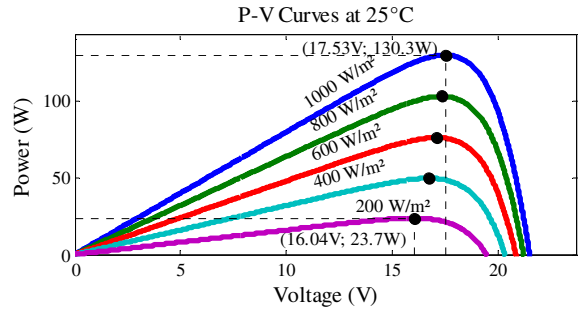


Figure 9. P-V curves for different conditions of irradiation at 25°C

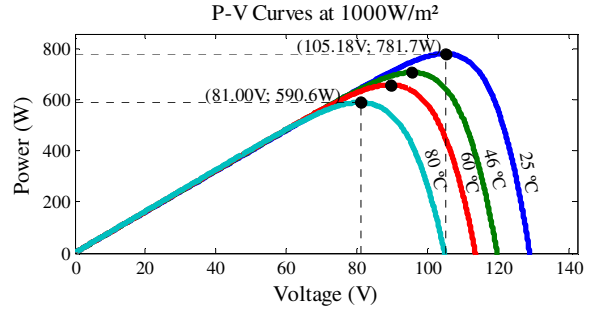


Figure 10. P-V Curves for different conditions of temperature for an irradiation of 1000 W/m^2

As shown before, the phase-controlled inverter imposes a voltage as a function of the trigger angle. Therefore, the maximum power point tracking (MPPT) must act on the trigger angle, so the converter's voltage is adjusted to work on a point of maximum power.

As the proposed converter presents limits of operation (angles from 120° to 180°), it will be made an analysis of the panel's voltage values for different conditions of irradiation and temperature. These results are compared to the normalized V_{DC} voltage of the converter (Figure 11).

Figure 9 shows the variation of voltage is low for low irradiation changes. For an irradiation of 200 W/m^2 , voltage at the maximum power point is 16.04V and for 1000 W/m^2 it is 17.53 V, it corresponds to a variation of 8.5%.

Figure 10 shows that changes on the panel's temperature imply in higher variations on voltage. For 80°C , the output voltage is 13.50V. This corresponds to a variation of 23% in comparison to 25°C .

TABLE II presents the output voltage of a panel for certain conditions of irradiation and temperature.

TABLE II. PANEL'S VOLTAGES AS A FUNCTION OF TEMPERATURE AND IRRADIATION.

Irradiation (W/m^2)	Voltage (V) 25°C	Voltage (V) 46°C	Voltage (V) 80°C
1000	17.54	15.97	13.51
800	17.38	15.79	13.30
600	17.14	15.54	13.01
200	16.05	14.37	11.71

TABLE III presents normalized voltages in comparison to the best situation (25°C a 1000W/m²).

TABLE III. NORMALIZED VOLTAGES AS A FUNCTION OF TEMPERATURE AND IRRADIATION

Irradiation (W/m ²)	Voltage (%) 25 °C	Voltage (%) 46 °C	Voltage (%) 80 °C
1000	100.00	91.05	77.02
800	99.09	90.02	75.83
600	97.72	88.60	74.17
200	91.51	81.93	66.76

At TABLE III it is possible to observe the worst presented situation: the panel's voltage is 66.76% of the best case's voltage.

Depending on the grid's voltage and the panel's model it is necessary to associate panels in series to fit the voltage levels of the panels with the inverter's. For its properly operation, the inverter's trigger angle must be lower than 180° so that, at the trigger's moment, the SCRs will be directly polarized. For this reason, the point of operation for maximum voltage needs to be chosen so the trigger angle stands below 180°. On this case, the 175° angle was chosen to obtain voltage at the best panel's operation situation. The worst, which corresponds to 66.76%, will take place with a trigger angle of 132°.

Figure 11 presents the curves for the normalized voltage of the converter.

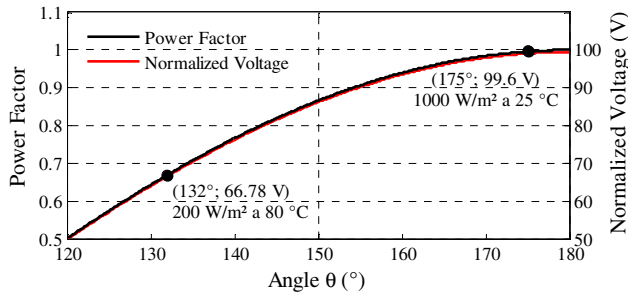


Figure 11. Voltage V_{DC} and power factor as a function of the trigger angle α .

Comparing the results from the table with the converter's waveforms, presented at Figure 11, the power factor will be 0.699 for a shooting angle of 132° and 0.996 for a trigger angle of 175°. Depending on the point of operation, it may occur losses at the power factor, however, the injected energy is capacitive, which can be useful for the electrical grid.

V. MAXIMUM POWER POINT TRACKING (MPPT)

As this converter is associated to photovoltaic cogeneration, it is necessary that it makes the maximum power point tracking (MPPT). Reference [10] presents some MPPT technics. The Perturb and Observe method, or P&O, was chosen due to it's simple technique. Other methods can normally operate. Figure 12 presents the implemented algorithm flowchart.

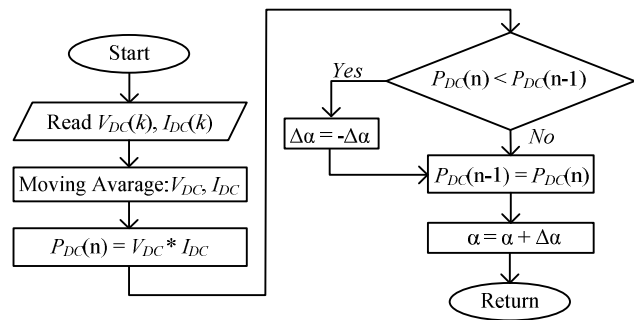


Figure 12. Perturb and Observe algorithm.

Due to the voltage and current ripples, it is necessary to develop the calculation of the moving average of the input acquired parameters I_{DC} and V_{DC} . The minimum time for the moving average calculus is a grid cycle, therefore, after the perturbation, the MPPT algorithm needs to wait until the calculation is over to make a decision.

VI. DEVELOPED PROTOTYPE

To validate the mathematical analysis, a prototype of the converter was built accordingly to specifications presented at TABLE IV. Figure 13 shows this prototype. The prototype has been designed to process 2340 W, which corresponds to the power of eighteen panels (number of panels available in the laboratory). Due to the limited quantity of panels available at the laboratory, the grid's connection voltage will be reduced. A PV emulator developed in the laboratory was used, providing a maximum power of 1389 W. The power is reduced due to hardware limitation. TABLE IV shows the nominal conditions of the inverter. The tests were performed with a reduced power.

TABLE IV. NOMINAL SPECIFICATIONS OF THE CONVERTER

Grid's phase-voltage (RMS) (V_A)	51,1 V
Grid frequency (f_{grid})	60 Hz
Number of photovoltaic panels	18
Number of panels connected in series	6
Maximum power for each panel	130 W
Maximum power provided by the system (P_{DC})	2340 W
Panel's voltage fo a 175° angle (V_{DC})	105,2 V
Current provided by each inverter (I_{DC})	8,02 A

As the current injected on the grid needs to complies with IEEE 519-1992 standards [11], a high-frequency filter have been included to the system. The project of this filter is presented at [12].

TABLE V. HIGH-FREQUENCY FILTER PARAMETERS.

L_f	C_f	R_f
16 mH	10 μ F	7,5 Ω

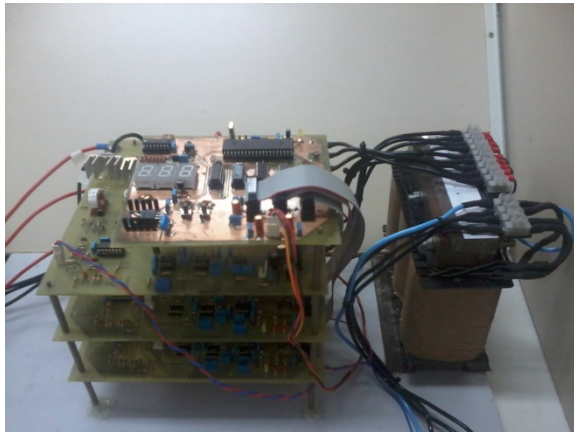


Figure 13. Experimental prototype.

VII. EXPERIMENTAL RESULTS

This section presents the results of the implemented prototype, where the panels were simulated by a photovoltaic panel's emulator developed at the laboratory. Due to the emulator's current limitation, the tests were managed with less power, the remaining parameters were chosen accordingly to TABLE V.

A. Steady-state results

This subsection presents the results with the converter operating in steady-state (without the MPPT interaction and variations at the operational conditions of the photovoltaic panels).

Figure 14 presents phase-voltages V_{R1} , V_{Rn} e V_R of the subsystems created by the autotransformer, showing the displacement between them is approximately 20° . The RMS values are 44.2V, 46.3V and 46.4V respectively.

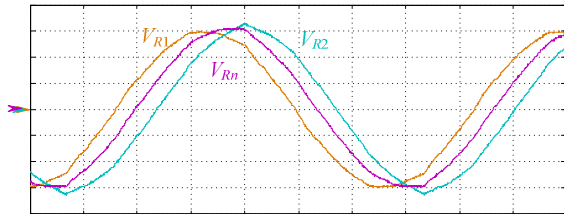


Figure 14. Voltage at phase R of the subsystems generated by the autotransformer.

Figure 15 presents input voltage and current for inverter 1. The average input current of this inverter is 4.44A and the average voltage for a 165° trigger angle is 104V. The voltage and current values for the remaining inverters are presented at TABLE VII.

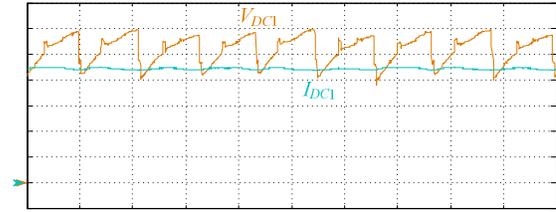


Figure 15. Input voltage and current of inverter 1 (1A/div, 20V/div, 2,5ms/div)

Voltage and current for phase R of inverter 1 are presented at Figure 16.

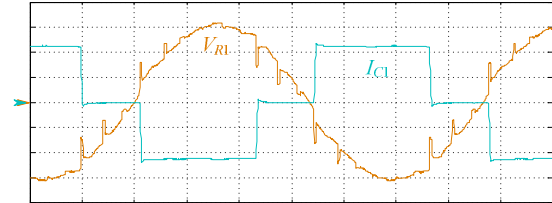


Figure 16. Voltage and current at phase R of inverter 1. (20V/div, 2A/div, 2,5ms/div)

Figure 17 presents voltage and current provided by phase A of the grid. This current has a THD of 9.03% experimentally obtained, before its passage by the filter.

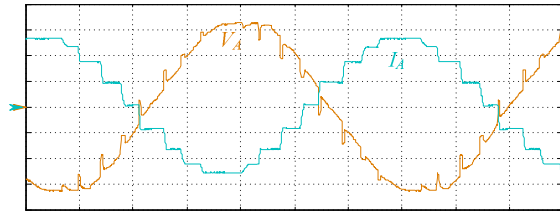


Figure 17. Output voltage and current for phase A of the autotransformer (20V/div, 5A/div, 2,5ms/div).

Figure 18 and Figure 19 present currents injected on the grid's three phases, after and before the passage by the filter, respectively.

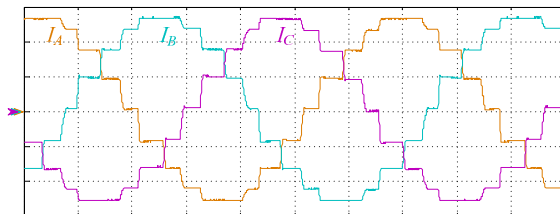


Figure 18. Currents of the three output phases of the converter (5A/div, 2,5ms/div).

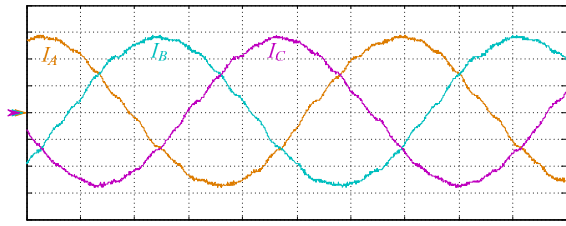


Figure 19. Currents injected at the three phases after passing through the filter (5A/div, 2,5ms/div)

The passage by the filter attenuates the undesirable harmonics and allows the converter to fit IEEE 519-1992 requirements. The harmonic analysis of this current will be presented at the next section.

The experimentally obtained results are presented at TABLE VI and TABLE VII.

TABLE VI. OUTPUT POWER FOR EACH PHASE.

Phase	Power (P)	Reactive Power (Q)	FP	Phase (α)
A	-442W	147VAR	-0.948	162.4°
B	-423W	135VAR	-0.953	163.2°
C	-413W	168VAR	-0.943	161.4°
Total	-1278W	428VAR	-	-
S _{Total}	1348VA			

TABLE VI presents the obtained output results for the three phases. TABLE VII shows input values for inverters 1, 2 and n . This converter has a measured efficiency of 97.04%.

TABLE VII. INPUT SPECIFICATIONS FOR EACH PHASE.

Inverter	V_{DC}	I_{DC}	P_{DC}
1	104V	4.44A	462W
2	106V	4.41A	467W
n	103V	4.47A	460W
Total	-	-	1389W

B. Operation with MPPT

This subsection presents tests with the MPPT operation. It is made 3 transitions in different conditions of operation of the panels, according to Figure 20. Curve A presents 200W/m² at 80°C, B has 600W/m² at 80°C and curve C 600W/m² at 25°C. The operation starts at point 1, after some time it is made the transition to point 2, and sequentially at point 3, ending at point 4.

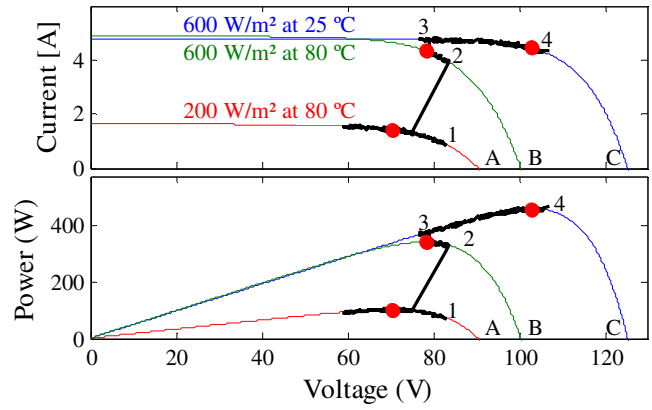


Figure 20. Operation of the MPPT method at inverter 1.

TABLE VIII. Results from tests of the inverter 1.

Curve	$I_{MPPT}(A)$	$V_{MPPT}(A)$	α (°)	FP	$I_{P_{MPPT}}(W)$
A	1.44	70.2	131	0.660	101.2
B	4.36	78.0	136	0.733	340.4
C	4.46	102.8	165	0.966	458.1

Figure 20 shows the converter track the maximum power point by the trigger angle variation at inverter 1. At curve A, the track presents a high oscillation due to the low current value, which injures the acquisition precision of the developed hardware.

The drawback of this technics is the power factor's reduction, due to the displacement variation between current and voltage. As the system has a capacitive reactive power supply, it can be absorbed by the grid, operating as a reactive compensator as well.

VIII. HARMONICS

Operating in normal conditions, without unbalances, just harmonics of $18k \pm 1$ orders do not complies the limits established by the IEEE 519-1992 standard. This problem can be solved with the addition of a high-frequency filter. Figure 21 presents a comparison between currents injected in the grid before using a filter and after the utilization of it.

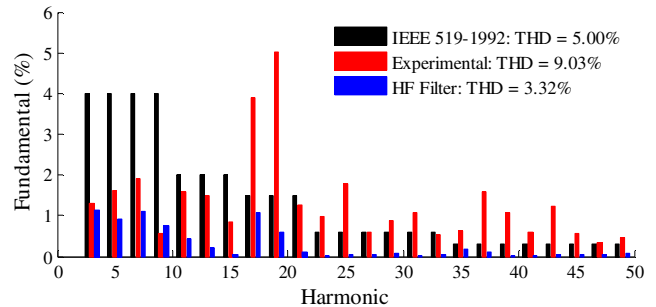


Figure 21. Harmonics of currents injected at the grid.

The experimental results present harmonics of different orders due to the input current's ripple. The dispersion reactance of the autotransformer and the grid make the experimental THD lower than the theoretical.

IX. CONCLUSION

This paper presents an alternative for the processing of energy generated by photovoltaic panels. The objective of this converter is to be installed at secluded places, where it is possible to obtain a high irradiation all year long and it does not require a constant maintenance, therefore, the desirable characteristics are: low-cost, robustness, reliability, easy maintenance, quality of the energy provided to the grid and the capacity of performing the track of the maximum power provided by the panels.

The elements which compose this converter (phase-controlled inverter and autotransformer) ensuring reliability, robustness and low-cost, as they are already consolidated technologies.

The converter is capable to track the maximum power acting on the panel's mean voltage. When the solar panel is operating on a point of maximum power and the irradiation or temperature varies (e.g.: shadowing), the power provided is reduced, thus, it is necessary to change the input voltage by the trigger angle until a point where the panel returns to provide maximum power for this new condition.

The studies presented the effect of a variation of temperature and irradiation on the panel's voltage, because the converter acts on it. The extreme analyzed situations were 1000 W/m² at 25 °C and 200 W/m² at 80 °C. The converter is able to operate on these conditions of voltage, with a power factor variation of 0.996 to 0.669 respectively, injecting reactive power in the electrical grid.

The experimental results were made with reduced power due to limitations of the photovoltaic panel emulator. This results confirm the system works properly, injecting low THD current (9.03% without filter and 3.32% with filter), meeting the IEEE 519-1992 standard in nominal operations. The power factor depends on the maximum power provided by the panel, but the reactive energy is capacitive, which can be absorbed by the grid. Despite the loss in the power factor due to the operation of the MPPT, the advantages provided to robustness, low cost and high efficiency (97.04% obtained experimentally), make this converter a viable alternative to photovoltaic cogeneration by proposing the processment of a high power at a reduced cost in remote and difficult to access places.

REFERENCES

- [1] O. Wasynczuk, "Modeling and dynamic performance of a line-commutated photovoltaic inverter system," *Energy Conversion, IEEE Transactions on*, vol. 4, no. 3, pp. 337-343, Sep 1989.
- [2] A. Sarwar and M. Jamil Asghar, "Multilevel converter topology for solar PV based grid-tie inverters," in *Energy Conference and Exhibition (EnergyCon), 2010 IEEE International*, 2010.
- [3] D. A. Paice, *Power Electronics Converter Harmonics: Multipulse Methods for Clean Power*, Wiley-IEEE Press, 1996.
- [4] B. Wu, *High-Power Converters and AC Drives*, J. W. Proffio, Ed., 2006.
- [5] F. J. M. D. Seixas and I. Barbi, "A new 12 kW three-phase impulse high power factor AC-DC converter with regulated output voltage for rectifier units," in *Telecommunication Energy Conference, 1999. INTELEC '99. The 21st International*, 1999.
- [6] R. C. Fernandes, P. D. S. Oliveira and F. J. M. D. Seixas, "A Family of Autoconnected Transformers for 12- and 18-Pulse Converters - Generalization for Delta and Wye Topologies," *Power Electronics, IEEE Transactions on*, vol. 26, no. 7, pp. 2065-2078, July 2011.
- [7] A. Kempe and U. Schonwandt, "EMC of PV-plants with line-commutated inverters," in *Photovoltaic Specialists Conference, 1996. Conference Record of the Twenty Fifth IEEE*, 1996.
- [8] L. Lapolli Brighenti, L. G. Kremer, A. L. Batschauer and M. Mezaroba, "Phase-controlled inverters associated to a multi-pulse autotransformer applied to photovoltaic cogeneration," in *Power Electronics Conference (COBEP), 2013 Brazilian*, 2013.
- [9] M. Villalva, J. Gazoli and E. Filho, "Comprehensive Approach to Modeling and Simulation of Photovoltaic Arrays," *Power Electronics, IEEE Transactions on*, vol. 24, no. 5, pp. 1198-1208, May 2009.
- [10] T. Esumi and P. L. Chapman, "Comparison of Photovoltaic Array Maximum Power Point Tracking Techniques," *Energy Conversion, IEEE Transactions on*, vol. 22, no. 2, pp. 439-449, June 2007.
- [11] IEEE Std 519-1992, *IEEE Recommended Practices and Requirements for Harmonic Control in Electrical Power Systems*, 1993, pp. 1-112.
- [12] L. L. Brighenti, L. G. Kremer, A. L. Batschauer and M. Mezaroba, "Phase-Controlled Inverters Associated to a Multi-Pulse Autotransformer Applied to Photovoltaic Cogeneration," *Cobep*, 2013.